Structural evolution and hydrogen sulfide sensing properties of $NiTiO_3$-TiO_2 sol-gel thin films containing Au nanoparticles

Gaspera, Enrico Della; Pujatti, Mattia; Guglielmi, Massimo; Post, Michael L.; Martucci, Alessandro

Publisher's version / la version de l'éditeur:
Materials Science and Engineering B, 176, 9, pp. 716-722, 2011-03-12

Web page / page Web
http://dx.doi.org/10.1016/j.mseb.2011.02.027
http://nparc.cisti-icist.nrc-cnrc.gc.ca/npsi/ctrl?action=rtdoc&an=18525848&lang=en
http://nparc.cisti-icist.nrc-cnrc.gc.ca/npsi/ctrl?action=rtdoc&an=18525848&lang=fr

Materials Science and Engineering B 176 (2011) 716–722

Contents lists available at ScienceDirect

Materials Science and Engineering B

journal homepage: www.elsevier.com/locate/mseb

Structural evolution and hydrogen sulfide sensing properties of $NiTiO_3$–TiO_2 sol–gel thin films containing Au nanoparticles

Enrico Della Gaspera[a,*], Mattia Pujatti[a], Massimo Guglielmi[a], Michael L. Post[b], Alessandro Martucci[a]

[a] INSTM and Dipartimento di Ingegneria Meccanica Settore Materiali, Università di Padova, Via Marzolo 9, 35131 Padova, Italy
[b] Institute for Chemical Process and Environmental Technology, National Research Council of Canada, 1200 Montreal Road, Ottawa, Ontario, Canada K1A 0R6

ARTICLE INFO

Article history:
Received 29 November 2010
Received in revised form 27 January 2011
Accepted 25 February 2011

Keywords:
Nanocomposites
Optical properties
Sensors
Thin films
Sol–gel

ABSTRACT

Thin films composed of a matrix of titanium and nickel oxides, doped with gold nanoparticles have been prepared with the sol–gel method and annealed at different time/temperature combinations. Structural characterizations demonstrate the crystallization of nickel titanate and of TiO_2-rutile due to nickel capability to promote rutile crystallization over anatase. Optical characterizations show a tunable refractive index of the samples according to the Ti/Ni ratio, and a high amount of residual porosity even after high temperature annealing. Sensor functionality measurements were performed with H_2, CO and H_2S: high sensitivity for hydrogen sulfide detection has been proved, and the cross sensitivity to the other two gases can be tuned by controlling the nickel amount. For high Ni concentrations, the matrix is composed of $NiTiO_3$ and TiO_2-rutile, and no cross sensitivity is experienced. For lower Ni amounts, TiO_2-anatase starts to crystallize and the films become sensitive to H_2 and CO.

1. Introduction

Noble metal nanoparticles embedded within metal oxide matrixes have become of great interest in material science research, due to their unique optical, electrical and catalytic properties. Such materials have applications in different fields like sensing, catalysis, light harvesting. In the gas sensor field, optical sensors have become a very important research topic in the last decade, due to the possibility to tune the response of the device by variation of the analysis wavelength, enabling to overcome the intrinsic problems of poor selectivity of classical electrical sensors. This is particularly the case when the active material is doped with metal nanoparticles (NPs) which exhibit a localized surface plasmon resonance (LSPR) in the spectral range of interest, usually in the visible and near infrared regions [1].

Moreover, optical sensors allow to widen the range of operative parameters compared to electrical sensors: in fact variation in intensity, frequency, polarization and phase of the transmitted/reflected light can be analyzed, and this can in principle improve the device performances by lowering the cross sensitivity between different gases.

Thin films of transition metal oxides (for example, SnO_2, WO_3, TiO_2 just to name a few) have been investigated in the past years due to their optical and electrical properties that showed them as good candidates for applications like sensing [2–4], catalysis [5,6], electrochromism and optoelectronics [7]. As fundamental requirements for thin films to be used as gas sensors, they should present high surface area, because the sensing mechanism is a surface process, and a tailored porosity in order to maximize the active surface of the material and create an easy path for the gas to enter and the reaction products to exit the film [8]. Moreover the control of microstructure, crystalline phases and grains size of the active material is of paramount importance in order to improve the performances of the sensor. In this view, we present a systematic study on sol–gel thin films composed of TiO_2 and $NiTiO_3$ containing a dispersion of Au NPs and gas sensing tests for a high performance hydrogen sulfide sensor are then presented as a potential application, since in a previous study by our group [9], good sensing performances of similar nanocomposite thin films were shown. The main focus of this work is to discuss the influence of chemical composition and of time and temperature of the thermal treatments on the microstructure of the nanocomposites, and to relate the hydrogen sulfide sensing properties, in particular the cross sensitivity with CO and H_2, to the different crystalline phases present in the films.

2. Experimental procedure

The nanocomposite films were obtained by the sol–gel method: a detailed description of the synthetic route adopted and associated hazards has been reported elsewhere [9]. Briefly, a solution of nickel chloride hexahydrate dissolved in ethanol was mixed to

* Corresponding author. Tel.: +39 049 8275634; fax: +39 049 827505.
E-mail address: enrico.dellagaspera@unipd.it (E. Della Gaspera).

0921-5107/$ – see front matter © 2011 Elsevier B.V. All rights reserved.
doi:10.1016/j.mseb.2011.02.027

Table 1
List of sample series prepared and their nominal composition.

Sample	Ti/(Ti + Ni) molar	Ni/(Ti + Ni) molar
5T5N	0.5	0.5
6T4N	0.6	0.4
7T3N	0.7	0.3
8T2N	0.8	0.2
9T1N	0.9	0.1
1T0N	1	0

a previously prepared solution of titanium butoxide, acetylacetone and water in ethanol and stirred for 20 min. Before deposition, a tetrachloroauric acid ethanolic solution was added to the Ti–Ni solution in order to achieve a 5% molar Au content. All deposition were made by spin coating on either Si and SiO_2 substrates in the range 2000–4000 rpm for 30 s under nitrogen atmosphere to prevent the rapid reaction of the film precursors with atmospheric moisture. Three different thermal treatments were studied: a progressive annealing from 500 °C to 800 °C with 4 steps (increasing by 100 °C each step) and with 30 min isothermal at every step, and two isothermal annealing at 500 °C and at 600 °C up to 10 h.

Six series of samples were prepared, with increasing Ni amount in the starting solution from 0% (pure TiO_2) to 50% molar with respect to the Ti + Ni total amount (stoichiometric TiO_2:NiO = 1:1 sample); Au content was kept constant in every sample at 5% molar, again with respect to Ti + Ni moles. Table 1 shows name and nominal compositions of the different series of samples.

The films were characterized by X-ray diffraction (XRD) by using a Philips diffractometer equipped with glancing-incidence X-ray optics. The analysis was performed at 0.5° incidence, using CuK_α Ni filtered radiation at 30 kV and 40 mA. The average crystallite size was calculated from the Scherrer equation after fitting the experimental profiles.

The surface structure of the nanocomposite films has been investigated by scanning electron microscopy (SEM).

Transmittance at normal incidence and ellipsometry quantities Ψ and Δ have been measured using a J.A. Woollam V-VASE Spectroscopic Ellipsometer in vertical configuration, at three different angles of incidence (65°, 70°, 75°) in the wavelength range 400–1500 nm. Refractive index n, absorption coefficient k, and film thickness have been evaluated from Ψ, Δ and transmittance data using the WVASE32 ellipsometry data analysis software, fitting the experimental data with the Cauchy dispersion, Gaussian and Tauc–Lorentz oscillators for the non absorbing region, Au SPR peak and UV absorption edge, respectively.

Optical sensor functionality was studied by making optical absorbance measurements over the wavelength range 350 nm < λ < 800 nm using a custom-built gas flow cell coupled with a Varian Cary1E spectrophotometer. Details are reported elsewhere [10].

Films were exposed to: H_2 (1%, v/v), CO (1%, v/v) and H_2S (10 ppm, 100 ppm), all balanced in dry air, at a flow rate of about 0.4 L/min and at 350 °C operative temperature (OT). The substrate size was approximately 1 cm × 2 cm and the incident beam was normal to the film surface and covering a 6 mm × 1.5 mm section area.

3. Results and discussion

A systematic XRD study was carried out in order to better understand the crystallization processes and structural changes occurring inside the nanocomposite films with different annealing temperatures and times. First, samples were annealed isothermally at 500 °C and 600 °C up to 10 h. Table 2 reports the results for the six samples and the 3 crystalline oxides detected: TiO_2 in the rutile phase (JCPDS No. 87-0920), TiO_2 in the anatase phase (JCPDS No. 84-1286) and $NiTiO_3$ (JCPDS No. 76-0335). There was no NiO phase present, as expected, due to the Ni precursor amount never being predominant in the solutions, and in the sample with the highest Ni amount (5T5N) it is stoichiometric with Ti, thus leading to nickel titanate formation, as recently shown for $NiTiO_3$ powders obtained from a similar sol–gel method [11], even if in our case the crystallization is found to occur at slightly higher time/temperature combinations. Au diffraction peaks (JCPDS No. 04-0784) are evident in all samples for all thermal treatments, so they were not taken into consideration for these overall analyses. As reported in our previous publication [9], the presence of Au NPs promotes the overall crystallization of the matrix: thus diffraction peaks can be detected even at 500 °C if the annealing time is long enough, while all Au-free samples were almost amorphous even after 10 h of annealing, with the exception of low Ni content samples (0% and 10%), which show TiO_2 anatase peaks. At 600 °C after 30 min treatments, the crystalline phases are easily detectable in all Au-containing samples, while without the noble metal, annealing times of 1–2 h are needed to produce any evidence of crystalline oxides. Also, when the annealing time is increased, diffraction peaks become more intense and sharper, as a consequence of the expected crystal growth and of the increase of the crystalline fraction.

It is noteworthy to underline that the thermal reduction of Au ions inside sol–gel oxide matrix occurs at lower temperatures compared to the one used in our experiments, and the nucleation and growth processes are quite fast [12]. As a consequence, as soon as the samples are placed in the furnace at the desired annealing temperature, organic compounds start to pyrolise and Au nanocrystals precipitate: their presence is found to be a crystallization promoter for the transition metal oxides in the matrix. The noble metal NPs effect in promoting crystallization and growth of oxides nanoparticles has also been observed in the past, for example, for SnO_2 powders [13] and TiO_2 powders [14].

In addition to the isothermal annealing, also progressive treatments from 500 °C to 800 °C have been analyzed, as described in Section 2. Fig. 1 summarizes all the results evaluated from the diffraction patterns of the 6 samples. On the horizontal axis annealing temperature is reported, while the vertical axis presents the relative intensity of the main XRD peak of the crystalline phases detected, calculated as the ratio between the peak of interest and the most intense peak for every dataset. As reported before, being nickel content is always below 50% molar, no NiO has been found, so the diffraction peaks taken into consideration are the (1 0 1) reflection at 25.3°, the (1 1 0) reflection at 27.4° and the (1 0 4) reflection at 33.1° for TiO_2-anatase, TiO_2-rutile and $NiTiO_3$, respectively. The stoichiometric 5T5N sample shows only nickel titanate peaks, with intensity increasing with annealing temperature, even if a very small amount of TiO_2-rutile is formed at high temperature, possibly due to an unwanted excess of Ti precursor used to prepare the starting solution. Increasing Ti content up to 90% results in a progressive intensification of rutile peaks, while titanate peaks become less intense; nevertheless, for both these two phases, for higher annealing temperature the intensity of the peaks increases, suggesting a higher degree of crystallization. As far as anatase is concerned, for the pure TiO_2 matrix it is the only crystalline phase detected, even for 800 °C treatment; for 9T1N and 8T2N samples (and just detectable also for 7T3N) anatase starts to form at lower temperatures, but when the annealing temperature is increased, the TiO_2 matrix evolves into the rutile phase. At 800 °C anatase is no longer detectable in any of the Ni-containing films. So the presence of nickel promotes the crystallization of titanium oxide in the rutile phase even for a low amount of Ni, but when the titanium content is over 70%, a transition process from anatase to rutile is observed. As reported in the literature [15], rutile is stable when the crystalline size is larger than 35 nm, while for a lower crystal

Table 2
Crystalline phases detected for the 6 samples annealed isothermally at 500 °C and 600 °C from 30 min up to 10 h. Au NCs are detectable in all samples for all the annealing parameters studied, so they were not presented in this table.

Sample	Temperature (°C)	TiO_2-rutile	TiO_2-anatase	$NiTiO_3$
5T5N	500	Absent	Absent	Absent
	600	Absent	Absent	After 30 min
6T4N	500	Absent	Absent	After 10 h
	600	After 30 min	Absent	After 30 min
7T3N	500	After 10 h	Absent	After 10 h
	600	After 30 min	After 1 h[a]	After 30 min
8T2N	500	After 10 h	After 4 h	After 10 h
	600	After 30 min	After 30 min[a]	After 30 min
9T1N	500	Absent	After 30 min	Absent
	600	After 1 h	After 30 min	After 30 min
1T0N	500	Absent	After 30 min	Absent
	600	Absent	After 30 min	Absent

[a] Decreasing intensity with time.

size, anatase and brookite are thermodynamically favored: in the present samples, the presence of nickel is found to be a trigger to rutile crystallization, also for small TiO_2 crystals. Again, Au diffraction peaks do not undergo any significant change during thermal annealing, at least in the analyzed temperature range, so Au NPs are stable inside the oxide matrix and therefore the Au main diffraction peak was not taken into account for the plots reported in Fig. 1.

For all the samples and all the crystalline phases (with the exception of anatase in 8T2N and 9T1N samples, where crystals undergo structural changes with temperature) an increase of annealing temperature causes a sharpening of diffraction peaks, indicating crystal growth. This is clearly shown with the SEM images reported in Fig. 2a that refer to the 7T3N sample, stabilized at 500 °C and then progressively annealed at 600 °C and 700 °C. As additional support for the crystallization process, respective XRD patterns are reported in Fig. 2b, and crystallite size evaluated with the Scherrer relationship for the three crystalline phases detected (TiO_2-rutile, $NiTiO_3$ and Au, using, respectively, 27.4°, 33.1° and 38.2° diffraction peaks) are reported in Table 3. Considering that the magnification is the same for all the three SEM images, a clear grain growth can be noticed after higher annealing temperatures, as also confirmed from the narrowing of the diffraction peaks. Nevertheless, a considerable amount of residual porosity is detectable even after 700 °C, a fundamental requirement for samples to be used in gas sensing

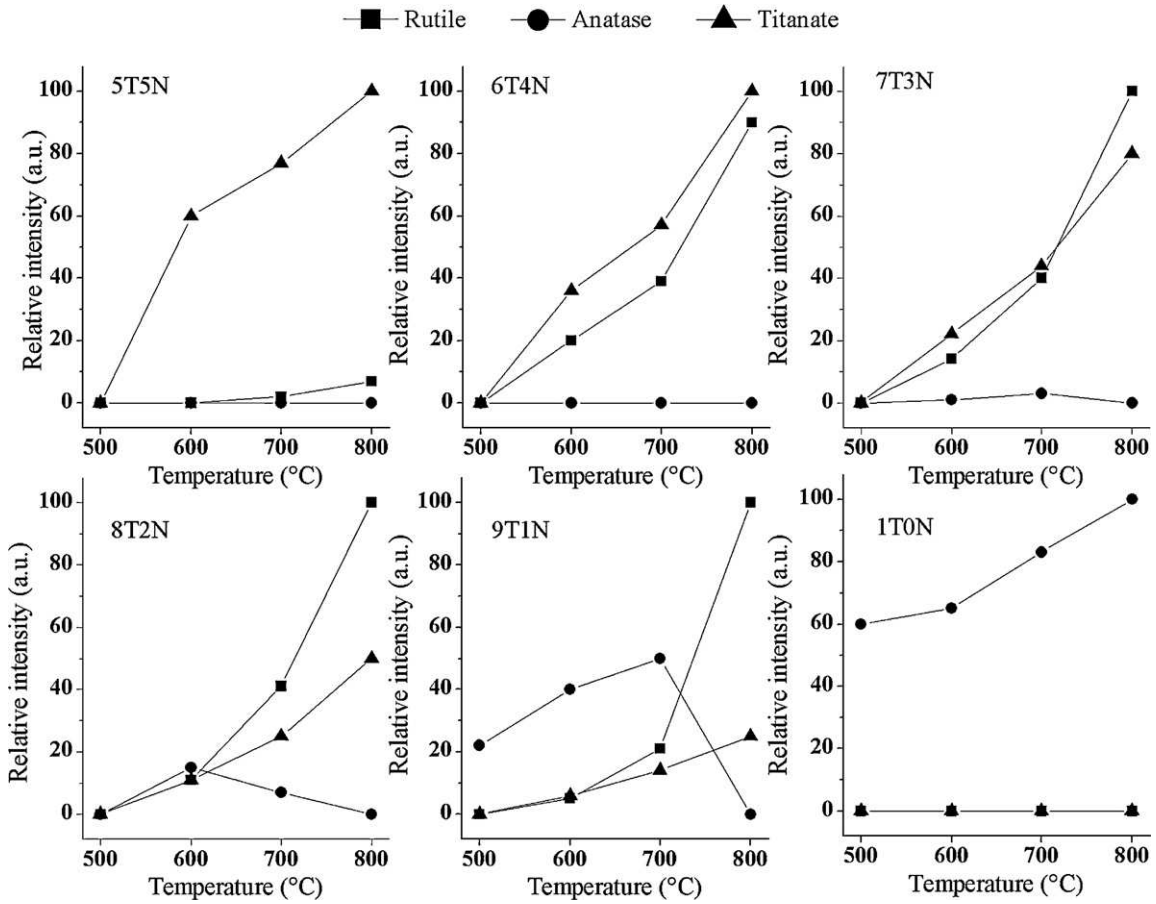

Fig. 1. Comparison between the relative intensity of the main diffraction peaks for TiO_2-rutile (■), TiO_2-anatase (●) and nickel titanate (▲), for the six Au-containing samples as a function of the annealing temperature. The Au diffraction peak intensity was not reported because it was almost insensitive to annealing temperature.

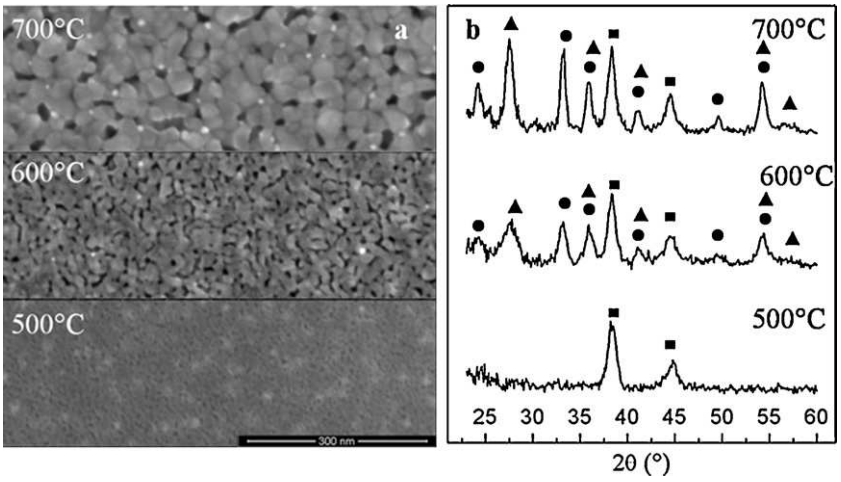

Fig. 2. (a) SEM micrographs of the 7T3N sample annealed at different temperatures. (b) Respective XRD diffraction patterns with highlighted Au (■), TiO_2-rutile (▲), and $NiTiO_3$ (●) peaks.

devices. In the high magnification imaging, also gold NPs as bright spots can be observed: they are statistically dispersed through the sample and no aggregation phenomena appear to occur.

Together with morphological and structural characterization, Au-containing samples were also optically characterized with optical absorption and spectroscopic ellipsometry in the UV–vis–NIR region. Refractive index dispersion curves versus wavelength for the six samples annealed at 500 °C are reported in Fig. 3a: a clear increase in refractive index together with Ti amount is observed, because of the higher value of rutile and anatase (2.51 and 2.7 at 590 nm, respectively [16]) compared to NiO (2.33 at 620 nm [17]) and $NiTiO_3$ (2.42 at 630 nm [18]). The dispersion curves are affected by the Au localized SPR band, that causes the perturbation between 600 nm and 800 nm as predicted by Kramers–Kronig relationship. For this reason, a comparison between refractive indexes has been done considering the values at 1100 nm, far enough from the Au-SPR region to be modeled with a Cauchy dispersion: results are reported in Fig. 3b, together with the SPR band position determined from the absorption spectra. As expected, an increase in refractive index causes a red shift of the plasmon band, although for some samples this effect seems more pronounced. Such behavior can be explained taking into account that the refractive index measured with ellipsometry is an average value, while the Au SPR band is affected from the matrix properties in the proximity of the particle surface. So it is likely that for some samples, the matrix has a slightly different composition, amount of crystallization, or porosity in close proximity to the gold particles compared to the average value, influencing the Au plasmon peak position.

Considering the tabulated refractive index values for the different oxides detected, and comparing them with the data measured with ellipsometry, it is evident that the experimental values for all the six samples are substantially lower than the expected values for a fully dense material of the same chemical composition. This difference is due to the residual porosity of the films that can be seen as an effective medium composed of dense materials and pores. Porosity was estimated by means of the Bruggerman relationship [19], considering as bulk material the film annealed at 1000 °C, even if a residual porosity also at that temperature cannot be totally excluded, and so the porosity determination is on the conservative side.

The 7T3N sample was annealed from 500 °C to 1000 °C with 30 min steps every 100 °C, and ellipsometric measurements have been performed at each step in order to calculate the refractive index evolution with annealing temperature. The obtained refrac-

Table 3
Mean crystallite diameter calculated according to the Scherrer equation for the diffraction peaks of 7T3N film annealed at 500 °C, 600 °C and 700 °C.

Temperature (°C)	Diameter (nm)		
	TiO_2-rutile	$NiTiO_3$	Au
500	–	–	11.5
600	6.5	11.7	11.2
700	11.2	18.5	12

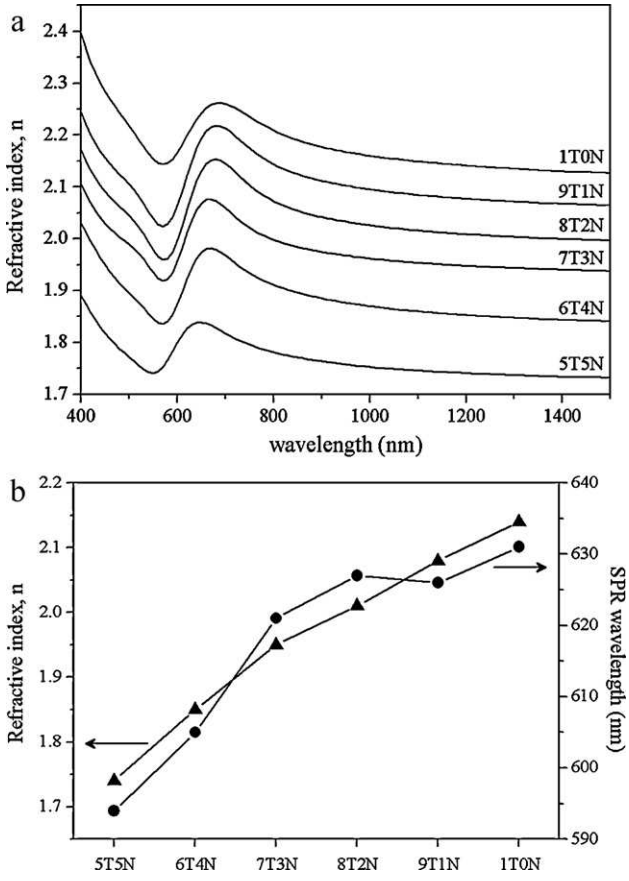

Fig. 3. (a) Refractive index dispersion curves for all the samples annealed at 500 °C. (b) Comparison between refractive index values measured at 1100 nm and the Au NPs SPR wavelength for the samples annealed at 500 °C.

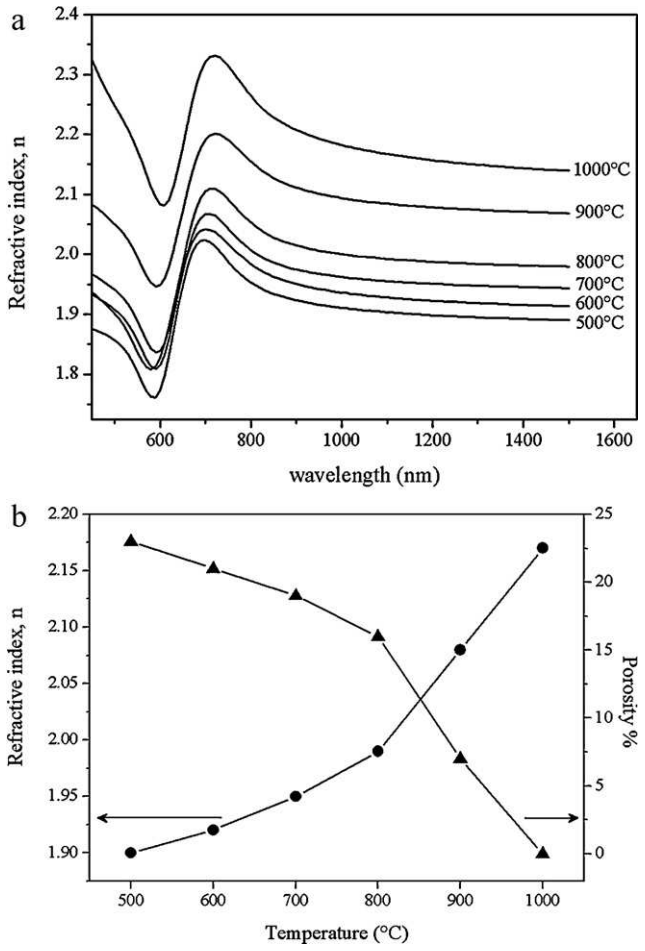

Fig. 4. (a) Refractive index dispersion curves for the 7T3N sample annealed from 500 °C to 1000 °C. (b) Evolution of refractive index and porosity with temperature for the same sample.

tive index dispersion curves are reported in Fig. 4a, where a clear increase in refractive index with temperature can be noticed, as a consequence of the decrease in porosity. Again, porosity determination was made by considering refractive index values at 1100 nm, far enough from Au SPR peak not to be affected by its absorption. Refractive index values at the different temperatures and porosity are reported in Fig. 4b.

Porosity of the nanocomposite films is in the range 16–23% up to an annealing temperature of 800 °C, then it decreases to 7% at 900 °C. As anticipated, this estimation is conservative because the film annealed at 1000 °C was chosen to represent a full dense material, even if its refractive index is lower than the theoretical value for a material composed of TiO_2-rutile and $NiTiO_3$, so a small amount of residual porosity is likely to be present in the sample annealed at 1000 °C.

Spectroscopic ellipsometry analysis is also helpful to measure sample thicknesses: a thickness decrease with increasing Ni amount was experienced, suggesting a role of Ni^{2+} ions in increasing solution viscosity by creating a complex with acetylacetone or promoting hydrolysis and condensation processes of titanium butoxide, since the precursor concentration and deposition parameters (spinning rate and time) were kept constant. The thickness of 500 °C annealed samples decreases almost linearly from about 200 nm to 100 nm when the Ni content is reduced from 50% to 0%.

These nanocomposites have been tested as optical sensors for hydrogen sulfide detection: all results reported in this section refer to samples stabilized at 500 °C and subsequently annealed at 600 °C,

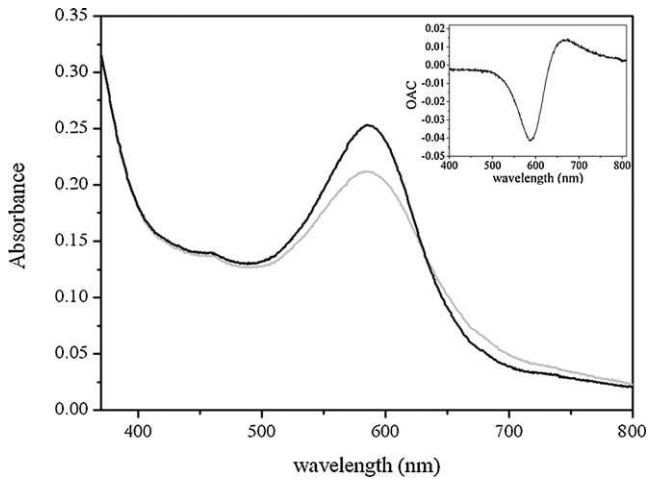

Fig. 5. Absorption spectra of the 5T5N film annealed at 600 °C measured in air (black line) and during exposure to 10 ppm H_2S (grey line) at the operative temperature OT = 350 °C. Inset: optical absorbance change (OAC = $A_{gas} - A_{air}$) of the same film.

because this thermal treatment was found to be a good compromise between porosity and crystallinity. Fig. 5 shows absorption spectra in the visible region for the 5T5N sample collected at 350 °C OT under dry air and under 10 ppm H_2S in dry air: a clear varia-

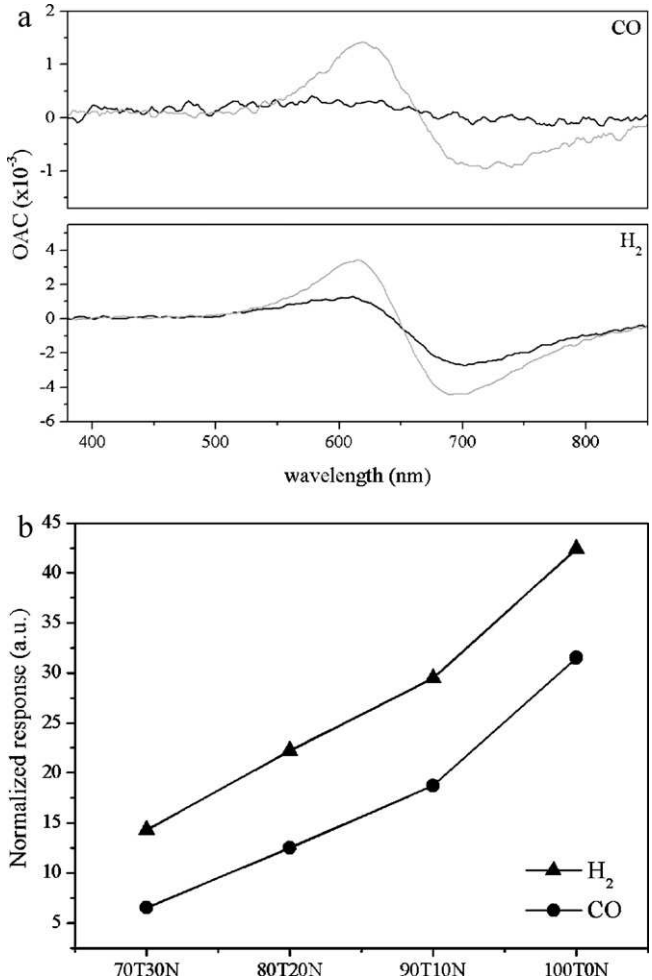

Fig. 6. (a) OAC curves for rutile-Au (black lines) and anatase-Au (grey lines) thin films when exposed to 1% CO or 1% H_2 in air. (b) Normalized response towards H_2 (▲) and CO (●) for the Ti-rich samples; data collected at the wavelength corresponding to the maximum of OAC curves for the two gases.

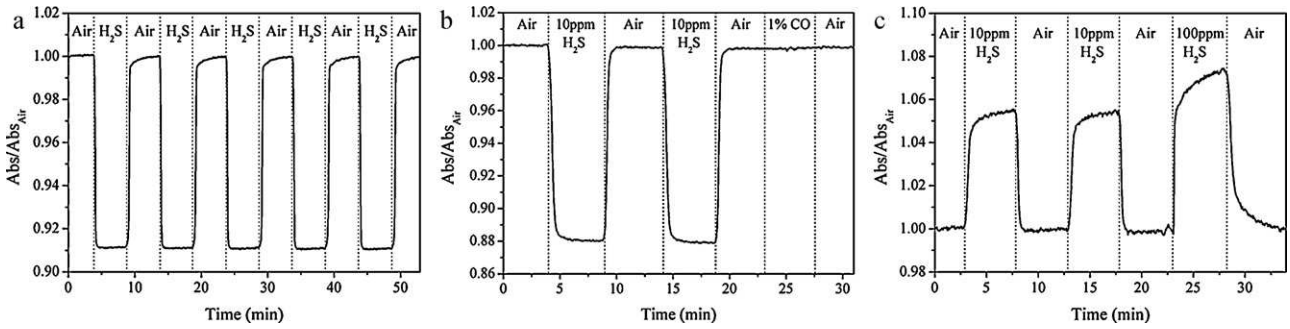

Fig. 7. (a) Dynamic response at 590 nm of the 5T5N nanocomposite film annealed at 600 °C under exposure to air–0.001% H_2S–air cycles at 350 °C OT. (b) Dynamic response at 605 nm of the 7T3N nanocomposite film annealed at 600 °C under exposure to air–0.001% H_2S–air–0.001% H_2S–air–1% CO–air cycle at 350 °C OT. (c) Dynamic response at 705 nm of the 7T3N nanocomposite film annealed at 600 °C under exposure to air–0.001% H_2S–air–0.001% H_2S–air–0.01% H_2S–air cycle at 350 °C OT.

tion in the Au SPR shape can be seen, with a decrease in intensity and a broadening of the peak. This variation is more clearly evident by plotting the optical absorption change ($OAC = Abs_{H_2S} - Abs_{air}$) versus wavelength, as reported in the inset: a strong absorbance decrease is found to occur in the range 500–630 nm, with the largest variation at 590 nm, while an increase in absorbance is seen at higher wavelengths, with a maximum at 670 nm. The observed change in absorbance is easily detectable with commercial spectrophotometers, that usually have a sensitivity better than 10^{-3}; moreover the error in these measurements is below 0.001, of the same order of magnitude of the instrument sensitivity. So in this OAC curve it is possible to identify two wavelengths corresponding to the two maxima (one negative and one positive) and also a range in which the sensor response is null, so giving various operative options in order to tune sensitivity and selectivity of the materials towards H_2S. By comparing the six samples, the behavior during hydrogen sulfide exposure is substantially the same, but the intensity of the response is different, being slightly smaller in the samples with lower amounts of nickel. This can be related to the decrease in sensor film thickness observed with lowering the nickel amount in the starting solution, as discussed above.

However, when the samples are exposed to 1% CO and 1% H_2, almost no response is observed, especially for nickel-rich samples, while a small response starts to appear for samples containing more than 70% of Ti precursor. This effect can be related to the presence of the anatase phase in samples with a lower amount of Ni, being the anatase-gold nanocomposites an already studied system for reducing gases detection [20]. Hence, nickel titanate and rutile are shown to be quite insensitive to carbon monoxide and hydrogen presence, even at high concentrations (1% i.e., 10,000 ppm). To prove that the two polymorphic structures of TiO_2 have different sensitivity towards CO and H_2, both Au-doped rutile and Au-doped anatase thin films of the same thickness and with the same Au amount have been prepared and tested at 350 °C OT with 1% CO and 1% H_2, and the results are presented in Fig. 6a. As would be expected, the rutile response to the two gases is lower compared to anatase, confirming the higher activity of the anatase phase for CO and hydrogen detection: this difference in sensitivity between anatase and rutile is demonstrated also in the nanocomposites containing $NiTiO_3$, as stated previously.

The difference in sensing performances of the two TiO_2 polymorphs has been proved also in the past, for example, analyzing the conductometric sensing response of TiO_2 thin films for H_2 detection: a much better response has been detected for anatase-based thin films, suggesting a key role played by the crystallographic phase in the sensing performances [21].

The progressive increase in sensitivity to hydrogen and CO when the Ti content is increased in the nanocomposite can be clearly seen in Fig. 6b. These data for the two gases are obtained by measuring the sensors response at the respective maxima of OAC curves, and the data have been normalized to the H_2S response value at the same wavelength. It is evident that the presence of anatase, due to the lower amount of nickel in the film, enables the nanocomposite to be sensitive also to the other two gases.

Analyzing the dynamic response behavior of the films subjected to repeated air–hydrogen sulfide–air exposure cycles, response times are in the range of few tens of seconds for all samples, as are the recovery times. A more rapid response performance is evident in samples with Ni content ranging between 50% and 30%. For lower nickel concentrations, the response and recovery times are still acceptable, but sometimes an incomplete retrieval of the baseline and a slightly unstable signal during gas flow appears. The observed differences can be related to the microstructure and the crystalline phases of the nanocomposite films.

In fact TiO_2 anatase, that crystallizes when Ni amount is lower than 30%, appears to be less efficient in decomposing the sulfide species on Au NPs, as suggested by the longer transient times and the drift of the optical absorption level when hydrogen sulfide is flowed for a prolonged period. On the contrary, when anatase is not present in the film, and so the matrix is composed only of rutile and nickel titanate, better sensing performances are experienced. An explanation of this behavior has been presented recently [22] in a study focused on the reaction between H_2S and the nanocomposite thin films: XPS and gaseous reaction product analyses have been performed, confirming the higher capability of $NiTiO_3$ in decomposing adsorbed sulfide species into sulfur oxides. Thus, samples with lower Ni content are more sensitive to carbon monoxide and hydrogen but they have a worse dynamic response towards hydrogen sulfide detection.

Fig. 7a shows the dynamic response of the 5T5N sample collected at 590 nm (negative maximum of OAC curve) when exposed to 5 cycles air–10 ppm H_2S–air: the behavior is almost ideal, with a square-like signal characterized by a great stability during gas flow and very fast transient times, with response and recovery times being 15 and 30 s, respectively, calculated as the time needed to reach 90% of the total signal change. The extremely good reversibility of the absorbance variation after the air–H_2S–air cycles can be appreciated. In Fig. 7b the dynamic performance of 7T3 N collected at the wavelength corresponding to the negative maximum of OAC curve is presented: the general performance is still good, only the response time is slightly longer (around 30 s) but there is no interference when 1% CO (1000 times the concentration of H_2S) is also flowed inside the test chamber, confirming the high selectivity properties of these nanocomposites. In Fig. 7c the temporal behavior of the same 7T3N sample collected at the wavelength corresponding to the positive maximum of OAC curve is illustrated: at this particular wavelength the effect of H_2S is to increase the absorbance, while at the operative conditions reported in Fig. 7b, H_2S causes a decrease in absorbance. This difference in the sign of the response allows the tuning of the sensor response by sim-

ply selecting the operative wavelength: this fact can be very useful especially when multiple gases analysis inside a mixture is needed.

4. Conclusions

Nanocomposite thin films with a matrix composed of Ti and Ni mixed oxides containing Au NPs have been synthesized using the sol–gel method. Structural morphology and crystallinity have been analyzed with XRD and SEM, confirming the role of nickel in promoting the crystallization of rutile TiO_2. Optical characterizations showed a tunable refractive index of the films according to the amount of Ti in the precursor, and revealed also a high amount of residual porosity of the samples. Optical sensing tests for hydrogen sulfide detection have been presented, showing excellent dynamic behavior and almost no interference with other reducing gases (CO, H_2), especially when the anatase phase of TiO_2 is absent, confirming high sensitivity and selectivity of these nancomposites towards H_2S, and the role played by the different oxides of the matrix in the sensing performances.

Acknowledgements

This work has been supported through the Progetto Strategico PLATFORMS (PLAsmonic nano-Textured materials and architectures FOR enhanced Molecular Sensing) of Padova University. E.D.G. thanks Fondazione CARIPARO for financial support. This article is recorded by National Research Council of Canada, NRCC# 52227.

References

[1] M. Ando, T. Kobayashi, M. Haruta, Catal. Today 36 (1997) 135–141.
[2] G. Korotcenkov, Sens. Actuators B 107 (2005) 209–232.
[3] G. Eranna, B.C. Joshi, D.P. Runthala, R.P. Gupta, Crit. Rev. Solid State Mater. Sci. 29 (2004) 111–188.
[4] N. Pinna, G. Neri, M. Antonietti, M. Niederberger, Angew. Chem. Int. Ed. 43 (2004) 4345–4349.
[5] T. Kawahara, Y. Konishi, H. Tada, N. Tohge, J. Nishii, S. Ito, Angew. Chem. Int. Ed. 41 (2002) 2811–2813.
[6] A. Bielanski, J. Haber, Catal. Rev. 19 (1979) 1–41.
[7] P. Bonhôte, E. Gogniat, M. Grätzel, P.V. Ashrit, Thin Solid Films 350 (1999) 269–275.
[8] G. Korotcenkov, V. Brinzari, A. Cerneavschim, M. Ivanov, V. Golovanov, A. Cornet, J. Morante, A. Cabot, J. Arbiol, Thin Solid Films 460 (2004) 315–323.
[9] E. Della Gaspera, M. Guglielmi, S. Agnoli, G. Granozzi, M.L. Post, V. Bello, G. Mattei, A. Martucci, Chem. Mater. 22 (2010) 3407–3417.
[10] A. Martucci, M. Pasquale, M. Guglielmi, M.L. Post, J.C. Pivin, J. Am. Ceram. Soc. 86 (2003) 1638–1640.
[11] M.R. Mohammadi, D.J. Fray, Solid State Sci. 12 (2010) 1629–1640.
[12] S. Sakka, H. Kozuka, J. Sol–Gel Sci. Technol. 13 (1998) 701–705.
[13] B. Bahrami, A. Khodadadi, M. Kazemeini, Y. Mortazavi, Sens. Actuators B 133 (2008) 352–356.
[14] A.A. Ismail, D.W. Bahnemann, I. Bannat, M. Wark, J. Phys. Chem. C 113 (2009) 7429–7435.
[15] H. Zhang, J.F. Banfield, J. Phys. Chem. B 104 (2000) 3481–3487.
[16] D.R. Lide, Handbook of Chemistry and Physics, 72nd ed., CRC Press, 1991, pp. 4–108.
[17] R.J. Powell, W.E. Spicer, Phys. Rev. B 2 (1970) 2182–2193.
[18] D.J. Taylor, P.F. Fleig, R.A. Page, Thin Solid Films 408 (2002) 104–110.
[19] D.A.G. Bruggerman, Ann. Phys. (Leipzig) 24 (1935) 636.
[20] D. Buso, M.L. Post, C. Cantalini, P. Mulvaney, A. Martucci, Adv. Funct. Mater. 18 (2008) 3843–3849.
[21] M. Epifani, A. Helwig, J. Arbiol, R. Diaz, L. Francioso, P. Siciliano, G. Mueller, J.R. Morante, Sens. Actuators B 130 (2008) 599–608.
[22] E. Della Gaspera, M. Guglielmi, G. Giallongo, S. Agnoli, G. Granozzi, F. Quaglio, A. Martucci, Sens. Lett. 9 (2011) 591–594.